INSTITUTE OF PHYSICS PUBLISHING JOURNAL OF PHYSICS D: APPLIED PHYSICS

J. Phys. D: Appl. Phys. **37** (2004) 307–317 PII: S0022-3727(04)67491-2

Microstructure and effective properties of nanocomposites: ferrofluids as tunable model systems

R Pelster, A Spanoudaki[1] and T Kruse

II. Physikalisches Institut der Universität zu Köln, Zülpicher Straße 77, 50937 Köln, Germany

E-mail: rolf.pelster@uni-koeln.de

Received 12 August 2003
Published 14 January 2004
Online at stacks.iop.org/JPhysD/37/307 (DOI: 10.1088/0022-3727/37/3/001)

Abstract

We have studied the correlation between microstructure and effective material properties using colloidal dispersions of magnetic nanoparticles in a carrier liquid (ferrofluids). Their microstructure can be altered in a continuous and reversible way via an external magnetic field. Two-dimensional small angle x-ray scattering and Monte Carlo simulations show that field-induced structural anisotropy develops due to the formation of anisometric particle clusters having a preferred orientation parallel to the field. In this polydisperse system particles of all sizes take part in cluster formation. The structural data are compared with results of dielectric measurements in the frequency range from 5 Hz to 1 GHz. We show that dielectric anisotropy is correlated with the shape anisometry of oriented clusters.

1. Introduction

The request for materials with specific mechanical, electrical and chemical properties has led to the development of composite materials combining the diverse characteristics of their components. Carbon fibre reinforced plastics, for example, that are used for building the outer structure of modern aircraft, combine low weight and high mechanical stability. In addition, their high conductivity results in good electromagnetic shielding and thus limits possible interference with electronic equipment [1]. But a straightforward prediction of effective material properties is only possible for rather simple microstructures. For example, consider a binary mixture, i.e. a material of permittivity ε_p dispersed in a matrix of permittivity ε_m. It can be considered as a so-called effective medium with homogeneous material properties as long as the wavelength of an applied electric field E is large compared with the length scale of its structural inhomogenities (e.g. particle diameters and interparticle distances). The measured effective permittivity is defined in terms of the average electric fields in the respective components. For an isotropic material this definition reads [2, 3]

$$\varepsilon_{\text{eff}} = \frac{(1-f)\varepsilon_m + f\varepsilon_p\langle E\rangle_p/\langle E\rangle_m}{(1-f) + f\langle E\rangle_p/\langle E\rangle_m}, \tag{1}$$

where $f = V_p/V_{\text{total}}$ denotes the volume filling factor of the dispersed component. Every change of microstructure leads to a change of the field distribution and thus of $\langle E\rangle_p/\langle E\rangle_m$ (see figure 1). Note that heterogeneity affects not only permittivity values but also determines the observable characteristic frequencies of polarization processes [4] and of molecular relaxations [5]. On the other hand, effective medium theory does not describe additional interface-induced mechanisms, such as altered molecular interactions at internal surfaces or confinement effects. But of course, such deviations can be detected [5].

There is a multiplicity of approximate effective medium formulas applying to different geometries [6, 7], whereas it is sometimes difficult to assess the respective range of validity. In the following, we focus on particles dispersed in a continuous host matrix (matrix inclusion or cermet topology). There are a few exact solutions of the so-called effective medium problem for simple systems like perfectly ordered arrangements of equal sized spheres or spheroidal particles [8–10]. An exact analytical solution for an arbitrary spatial configuration of

[1] Present address: Laboratory of dielectric spectroscopy, Department of Applied Mathematics and Physics, National Technical University of Athens, Zografou Campus 15780, Greece.

well-separated spheres has been formulated in [11]. On its basis we have performed three-dimensional-computer simulations and were able to show that two of the well-known effective medium formulas for randomly dispersed particles describe the limits of very narrow and very broad particle size distributions, at least up to filling factors of about 30%: for monodisperse spheres the Maxwell–Garnet formula holds, while for polydisperse systems with a sufficiently broad size distribution the Hanai–Bruggeman formula applies [12]. The latter is often successfully applied to describe experimental data since most real systems are polydisperse (see, e.g. [5]). But of course, depending on the degree of agglomeration real systems can show more complicated non-random spatial arrangements (see, e.g. figure 1 in [4]).

A better knowledge of the above correlation between structure and effective properties is indispensable for both correct interpretation of macroscopic measurements and tailoring of composite materials. Experiments on systems of dispersed particles can help, but it is difficult to compare samples that differ regarding the spatial arrangement as well as shape and size distribution of particles. For this reason we have chosen a model system: ferrofluids consisting of magnetic nanoparticles in a carrier liquid. Their microstructure can be altered in a continuous and reversible way via an external magnetic field, while components and mixture ratio remain unchanged. We have studied the field-induced orientation/formation of anisometric particle clusters by means of two-dimensional small angle x-ray scattering (2D-SAXS) and Monte Carlo simulations [13, 14]. The structural data are now compared with results of dielectric measurements in the frequency range from 5 Hz to 1 GHz in order to correlate structural and dielectric anisotropy.

2. Ferrofluids

2.1. A short overview

Ferrofluids are colloidal dispersions of magnetic monodomain nanoparticles in a carrier liquid [15, 16]. The particles are either charged or coated with a surfactant layer to prevent the formation of permanet agglomerates (so-called ionic and surfacted ferrofluids). In a magnetic field, the magnetic moments of the particles tend to orient themselves parallel to the field direction. When an external magnetic field is applied, ferrofluids develop anisotropic properties, e.g. dielectric [17–19] or optical [20, 21] anisotropy. It is evident that this must be due to a field-induced anisotropic microstructure, i.e. due to the presence of non-spherical units (single particles or clusters) having an orientation parallel to the applied magnetic field. In fact, anisometric clusters have been observed in x-ray studies [13, 22] as well as in computer simulations of monodisperse systems [23].

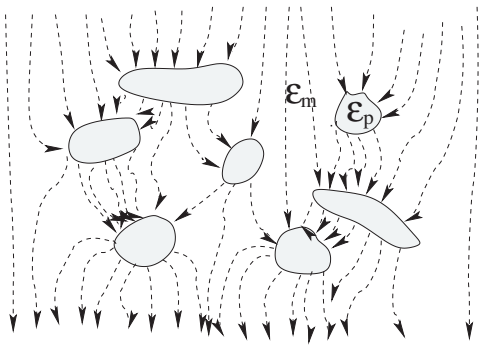

Figure 1. Qualitative raw sketch of inhomogeneous field distribution in a system of particles dispersed in a matrix (respective permittivities ε_p and ε_m). Shape and size distribution of particles as well as their spatial arrangement affect the field distribution and thus the measured effective permittivity (see equation (1)).

2.2. Samples

We purchased surfacted ferrofluids from Ferrofluidics GmbH (Nürtingen, Germany). They contain magnetite (Fe_3O_4) particles dispersed in Isopar-m, an oil. The particles have a mean diameter of about 10 nm. TEM investigations show that they deviate only little from spherical shape [24], a result that is confirmed by 2D-SAXS measurements revealing an effective axis ratio of 1.05 [13, 25]. The particles are covered with a surfactant layer consisting of oleic acid spacer molecules having a chain length of about 2 nm. The samples studied are listed in table 1. The volume fraction, f, of magnetite particles has been calculated directly from density measurements using a standard procedure.

Let us denote the respective volume filling factors and densities of our three-component system as f, ρ (magnetite particles), f_s, ρ_s (surfactant) and f_c, ρ_c (carrier liquid). Then, for the density of the ferrofluid $\rho_{FF} = f \cdot \rho + f_s \cdot \rho_s + f_c \cdot \rho_c$ holds. With $f + f_s + f_c = 1$ we thus obtain

$$f = \frac{\rho_{FF} - \rho_c}{\rho - \rho_c} + \underbrace{\left(f_s \cdot \frac{\rho_s - \rho_c}{\rho - \rho_c} \right)}_{<0.01}. \qquad (2)$$

This equation is also valid when the carrier liquid contains a certain amount of excess surfactant (f_s denotes the volume filling factor of all surfactant molecules in the sample). The second term on the right side can be neglected since the densities of surfactant and carrier liquid are similar. With $\rho_s \simeq 0.895\,\mathrm{g\,cm^{-3}}$, $\rho_c = 0.78\,\mathrm{g\,cm^{-3}}$, $\rho = 5 \pm 0.1\,\mathrm{g\,cm^{-3}}$ [26, 27] and an upper limit of $f_s < 0.5$, we can estimate that it only yields a contribution of at most 0.01. As a consequence, it is possible to evaluate the particle filling factor, f, even when the exact amount of surfactant is not known, e.g. when the carrier liquid contains some excess surfactant. We have measured both the density of the carrier liquid, ρ_c, and the overall

Table 1. Saturation magnetization, M_S (specified by Ferrofluidics), and volume fraction, f, of magnetite as determined by density measurements (the values in parenthesis are the producer's specification, yielding too low values, see text).

Ferrofluid samples (Ferrofluidics GmbH)			
Sample	M_S (mT)	f(%)	
Isopar-m	0	0.0	(0.0)
EMG 912	5	0.9	(0.9)
EMG 911	10	2.4	(1.7)
EMG 909	20	4.8	(3.6)
EMG 905	40	9.9	(7.1)
EMG 901	60	13.0	(10.7)
EMG 901a	60	15.0	(10.7)
EMG 900	90	19.0	(16.3)

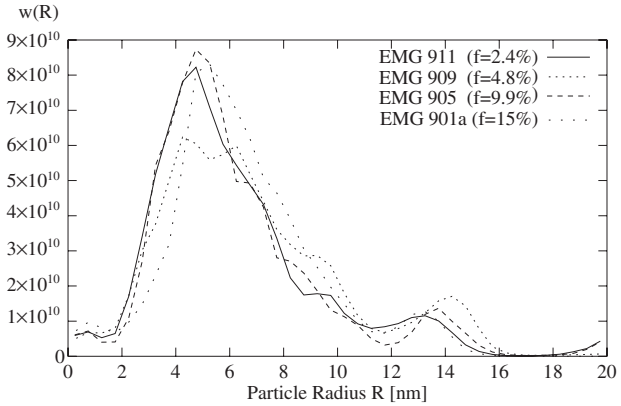

Figure 2. The volume-weighted size distribution of the magnetite particles as a function of particle radius.

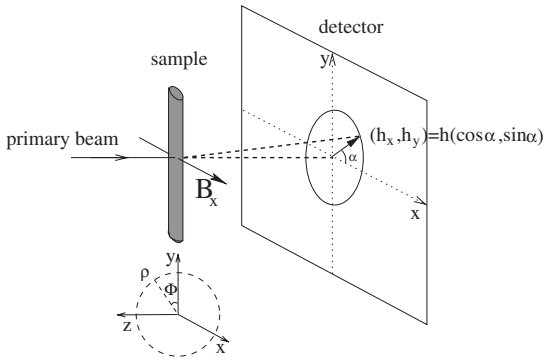

Figure 3. The geometry of the 2D-SAXS measurements, where the samples are exposed to a homogeneous magnetic field. For the spatial coordinates we use both a Cartesian and a cylindrical system $[(x, y, z)$ and $(x, \rho, \Phi)]$.

density of the ferrofluid, ρ_{FF} (for details see [13]). Using the literature value for the density of magnetite, ρ, we obtain filler fractions in the range from 0% to 19% for our samples (see table 1). Note that the manufacturer's specification gives too low values since they are calculated as the ratio of the sample's saturation magnetization $M_{\mathrm{S}} = (B - \mu_0 H)_{\mathrm{s}}$ to that of bulk magnetite, $f = M_{\mathrm{S}}/M_{\mathrm{bulk}}$. This procedure is only correct in cases where the mean saturation magnetization of a particle, M_{p}, equals that of the bulk material. But it is known that for nanoparticles $M_{\mathrm{p}} < M_{\mathrm{bulk}}$ holds, probably due to non-magnetizable surface layers [28] or lattice tensions [29]. We can confirm this observation: using our f-values we obtain a mean particle saturation magnetization of $M_{\mathrm{p}} = M_{\mathrm{S}}/f = 0.4025\,\mathrm{T}$ compared with $M_{\mathrm{bulk}} = 0.56\,\mathrm{T}$ [15].

For four of the samples we have also determined the size distribution of the particles via x-ray scattering and using the structure interference method [30, 31] (for details see [13]). Figure 2 shows rather broad size distributions with a maximum at a radius of about 4.5–5 nm and a half-width of about 4–5 nm.

3. 2D-SAXS: field-induced anisotropy and cluster composition

Four of the samples were selected for an x-ray study (EMG911, 909, 905 and 901a corresponding to filling factors $f = 2.4\%$, 4.8%, 9.9% and 15%, see table 1). The SAXS experiments took place at the JUSIFA beamline at Hazylab, DEZY, Hamburg [32] at energy $E = 7.09\,\mathrm{keV}$ (0.174 nm). The set-up for the two-dimensional experiments is sketched in figure 3. The samples were placed in capillary tubes and exposed to magnetic inductions, B, from 0 to 0.3 T, whereas the field direction, $\hat{x}$, was perpendicular to the beam direction, $-\hat{z}$. All measurements were conducted at room temperature. For more details we refer to [13, 25]. Figure 4 shows the two-dimensional scattered intensities at different magnetic fields for the sample EMG 905 ($f = 2.4\%$). At $B = 0$ the intensity pattern is isotropic; i.e. it does not depend on the direction of the scattering vector, $\vec{h}$ (see figure 3). With increasing magnetic field the intensity in the direction $\vec{h} \parallel \vec{B}$ decreases, while it increases in the perpendicular direction. Above a saturation induction of $B = 0.3\,\mathrm{T}$ the intensity pattern does not change any more. The observed anisotropy $I_{\vec{h}\parallel\vec{B}} < I_{\vec{h}\perp\vec{B}}$ reflects a change in microstructure that is reversible.

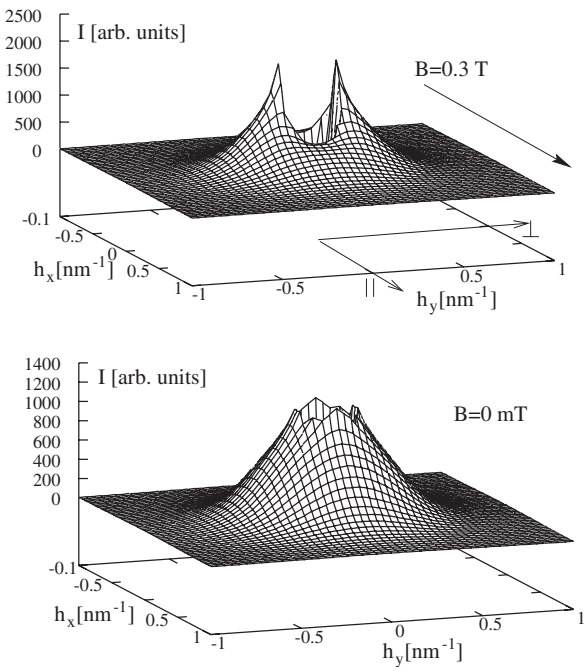

Figure 4. Field-dependent intensity pattern for sample EMG 905. There are no data at small scattering vectors, $|h| < 0.15\,\mathrm{nm}^{-1}$, since in this region the intensity of the primary beam dominates.

In order to get further information on these field-induced particle re-arrangements, we proceed with a quantitative analysis of the intensity patterns. Let I_{e} be the scattering intensity of a single electron. The intensity scattered in a volume V of a sample,

$$I_{B;h\neq 0} = I_{\mathrm{e}} \int \gamma_B(\vec{r}) \cos(h_x x) \cos(h_y y)\, \mathrm{d}V, \qquad (3)$$

depends on the electron density contrast between magnetite particles and carrier liquid: the characteristic function or autocorrelation function $\gamma(\vec{r}) = \Delta\varrho_{\mathrm{e}}(\vec{r}) * \Delta\varrho_{\mathrm{e}}(-\vec{r})$ is the convolution of the electron density contrast, i.e. of the difference between local electron density at a point $\vec{r}$ and its volume average, $\Delta\varrho_{\mathrm{e}} = \varrho_{\mathrm{e}}(\vec{r}) - \bar{\varrho}_{\mathrm{e}}$. The autocorrelation function contains information on characteristic particle distances. Above all, autocorrelation of next

neighbours is important in disordered systems such as ferrofluids. Note that γ is a two-dimensional function of cylindrical coordinates x and $\rho = \sqrt{y^2 + z^2}$ (see figure 3): at $B = 0$ the intensity pattern is isotropic, i.e. γ only depends on $|\vec{r}| = \sqrt{x^2 + \rho^2}$. On application of a homogeneous magnetic field, the intensity pattern becomes anisotropic since γ develops a cylindrical symmetry along the field axis, $\hat{x}$ (for details we refer to [13]).

We are interested in field-induced changes such as cluster formation and anisotropy. For this reason we evaluate the quantity $\Delta\gamma_B = \gamma_B - \gamma_{B=0}$: we calculate the difference of the measured two-dimensional intensity patterns with and without applied field, $I_B - I_{B=0} = I_e \int \Delta\gamma_B \cos(h_x x) \cos(h_y y)\, dV$, and invert the integral using a two-dimensional equidistant discretization of the $(\hat{x},\hat{\rho})$ space. The result is displayed in figure 5. For $B > 0$ we observe peaks located on the field axis at $x \simeq 10\,\text{nm}$ and $\rho = 0$. They indicate the existence of particle clusters having a preferred orientation parallel to the applied field. In order to show more clearly the development of anisotropy we divide $\Delta\gamma$ into an isotropic and an anisotropic part, whereas the latter one only contributes along the field direction: $\Delta\gamma_B(x, \rho) = \Delta\gamma_B^{\text{iso}}(\sqrt{x^2 + \rho^2}) + \gamma_B^{\text{aniso}}(x, 0)$ (since the autocorrelation function at zero field, $\gamma_{B=0}$, is isotropic, γ^{aniso} is also the anisotropic part of $\gamma_B = \gamma_B^{\text{iso}} + \gamma_B^{\text{aniso}}$). We have evaluated the anisotropic part $\gamma_B^{\text{aniso}}(x, 0) = \Delta\gamma_B(x, 0) - \Delta\gamma_B(0, x)$ and display it in figure 5(*b*) for different field strengths. With increasing magnetic field, anisotropy becomes stronger, i.e. there is an increasing number of clusters aligned parallel to the field. Either randomly orientated clusters orient themselves or new clusters form. For all field strengths and all samples we observe maximum autocorrelation at a distance of $x \simeq 10\,\text{nm}$. As mentioned above, the autocorrelation of next neighbours dominates in disordered systems, so that we can interpret the above value as mean centre-to-centre particle distance in oriented clusters, $\bar{d}_C \simeq 10\,\text{nm}$. As a consequence, for the mean radius of clustered particles

$$\bar{R}_C \leqslant \frac{\bar{d}_C}{2} \simeq 5\,\text{nm} \tag{4}$$

holds. The inequality is due to the finite surface-to-surface distance: it is caused by partially inter-penetrating surfactant layers and can be as small as 1 nm (see TEM studies in [24]). Surprisingly, this radius is of the order of the overall mean particle radius in the ferrofluid (see figure 2). Apparently particles of all sizes contribute to cluster formation. At first glance, this seems a contradiction, since the magnetic dipole–dipole interaction energy is size dependent (see below, equation (7)), so that mainly larger particles should form clusters [33, 34]. But our result shows that the picture of large agglomerating particles and small single particles is too simple. Obviously, a sufficiently large fraction of small particles takes part in cluster formation (for a detailed discussion of size dependent agglomeration probabilities we refer to [14]). There is another indication that there must be an additional energy involved: the dipole–dipole interaction energy of such small particles with $\bar{R}_C \leqslant 5\,\text{nm}$ would not be sufficient to guarantee thermal stability at room temperature [13]. Of course, there is no other comparable long-range interaction energy. But in a cluster, at surface-to-surface distances of the order of 1 nm, the short-range van der Waals energy (see equation (8)) can even exceed the dipole–dipole energy [13].

Summarizing, an analysis of our 2D-SAXS data shows a field-dependent change of microstructure due to orientation and/or formation of polydisperse clusters. These are composed of nanoparticles at short distances, so that both the magnetic dipole–dipole and the van der Waals energy contribute to thermal stability.

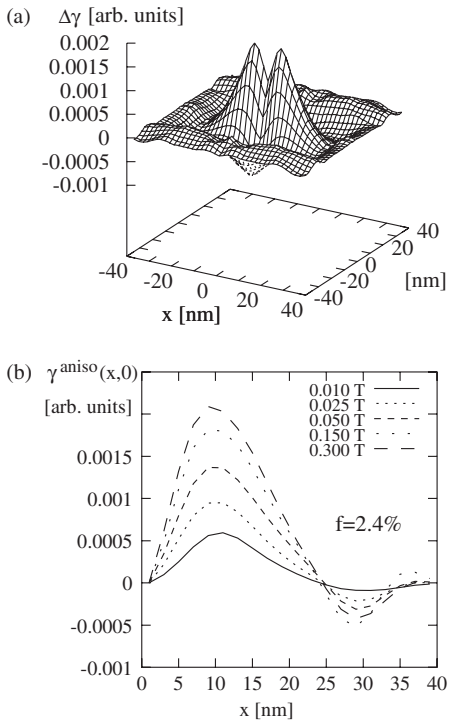

Figure 5. (*a*) Difference of characteristic functions with and without field, $\Delta\gamma = \gamma_B - \gamma_{B=0}$, for sample EMG911 and $B = 0.3\,\text{T}$. (*b*) Its anisotropic part along the field axis, $\gamma_B^{\text{aniso}}(x, 0) = \Delta\gamma_B(x, 0) - \Delta\gamma_B(0, x)$.

4. Monte Carlo simulations of polydisperse ferrofluids: the shape anisometry of clusters

Computer simulations of monodisperse systems [35] indicate that agglomeration behaviour strongly depends on the strength of dipole–dipole interaction and thus on particle size. But there are only a few studies of polydisperse systems [36]. To our knowledge there are no simulations of polydisperse sytems in the range $f = 0$–20% taking both the dipole–dipole and the van der Waals energy into account.

In order to get information on the orientation and/or formation of anisometric clusters that give rise to the aforementioned anisotropic microstructure, we have performed Monte Carlo simulations of four of our ferrofluids at room temperature. We assume the same mean particle magnetization $M_p = 0.4025\,\text{T}$ and use the respective filling factors and particle size distributions of samples EMG911, 909, 905 and 901a (see table 1 and figure 2) (for further details we refer to [14, 25]).

4.1. Model and algorithm

Depending on the concentration of the sample, 140–1300 particles are randomly distributed in a cubic cell of side length

100–150 nm (this is 20–25 times the mean particle radius). Following the Metropolis algorithm [37] the particles can perform random translation as well as rotation of their magnetic moments, as long as the probability for the corresponding change of potential energy is sufficiently high (i.e. as long as $\exp(-\Delta E_i/(k_B T) \geqslant q_i$ holds, where $q_i \in [0, 1]$ is a random number). When the total potential energy of all particles does not change significantly any more, thermal equilibrium is reached and the simulation stops.

The resulting spatial distribution of particles (equilibrium configuration) depends on their interaction, i.e. on (a) steric, (b) long-range magnetic dipole–dipole and (c) short-range van der Waals forces:

(a) Two particles of magnetic core radii R_i and R_j cannot overlap, so that for their minimum centre-to-centre distance at least $r_{ij}^{\min} \geqslant (R_i + R_j)$ holds. The smaller the particles, the lower the value of $r_{ij}^{\min}$. The surfactant layer prevents permanent agglomeration, increasing this minimum distance. The oleic acid molecules have a length of 2 nm but are not rigid rods and can be tilted or entangled. In addition, the inverted micelle structure of the surfactant layers leaves enough free volume for a partial inter-penetration of adjacent layers [38]. This is sketched in a simplyfied way in figure 6: the smaller a particle, the higher its surface curvature and the better the inter-penetration of adjacent surfactant layers. Of course, the closest approach will depend on the molecular details. Here we chose the most simple picture: with regard to steric interaction we model the particles as hard spheres of radius $1.1R_i$, i.e. in the simulation two particles are not allowed to approach closer than to a centre-to-centre-distance of

$$r_{ij}^{\min} = 1.1(R_i + R_j). \tag{5}$$

With this choice, particles of mean radius 5 nm can approach each other up to 1 nm, a value that is comparable with that observed in TEM studies [24]. Thus, the corresponding potential energy of steric interaction is

$$E_{ij}^{s}(r_{ij}) = \begin{cases} \infty & \text{for } r_{ij} < r_{ij}^{\min}, \\ 0 & \text{otherwise.} \end{cases} \tag{6}$$

(b) A particle i with magnetic moment $\vec{\mu}_i$ at position $\vec{r}_i$ will interact with the dipole field produced by a second particle j at $\vec{r}_j$. At a centre-to-centre distance $r_{ij} = |\vec{r}_j - \vec{r}_i|$ the magnetic dipole–dipole interaction energy is

$$E_{ij}^{dd}(r_{ij}) = \frac{\mu_0}{4\pi}\left(\frac{\vec{\mu}_i\vec{\mu}_j}{r_{ij}^3} - 3\frac{(\vec{\mu}_i\vec{r}_{ij})(\vec{\mu}_j\vec{r}_{ij})}{r_{ij}^5}\right). \tag{7}$$

For the magnetic dipole moment of monodomain nanoparticles $|\vec{\mu}_i| = (4/3)\pi R_i^3 M_p$ holds, where $M_p = 0.4025\,\mathrm{T}$ denotes the mean particle saturation magnetization (see section 2.2).

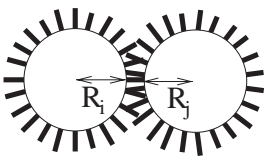

Figure 6. Sketch of two clustered particles. The partial inter-penetration of the surfactant layers defines a range of distances for which particles can be considered as clustered (see equation (13)).

Due to its size dependence, $\mu_i \propto R_i^3$, polydispersity may affect considerably the microstructure. In our simulations we therefore use ensembles of particles with a size distribution of log-normal shape fitting the actual size distributions of the samples (see figure 2 and [13]). In order to obtain a good statistical representation with a limited number of particles, we set $R_{\max} = 10\,\mathrm{nm}$. These bigger particles make up about 10% of the volume. The above procedure also avoids artificial giant dipole moments that do not exist in real ferrofluids since huge particles would not be magnetically monodomain.

(c) At close surface approach the short-range van der Waals interaction can be of the same order of magnitude as the dipole–dipole interaction [39]:

$$E_{ij}^{vd\,W}(r_{ij}) = -\frac{A_H}{6}\ln\left(\frac{r_{ij}^2 - (R_i + R_j)^2}{r_{ij}^2 - (R_i - R_j)^2}\right) - \frac{A_H}{6}\left[\frac{2R_iR_j}{r_{ij}^2 - (R_i + R_j)^2} + \frac{2R_iR_j}{r_{ij}^2 - (R_i - R_j)^2}\right]. \tag{8}$$

Here A_H denotes the Hamaker constant, the value of which depends on the dielectric properties of particles, surfactant and carrier liquid [40]. For Fe_3O_4 particles in kerosine (Isopar-m), A_H is of the order of magnitude of 10^{-19} J within an uncertainty factor of 3 [15,41]. With $A_H = 0.5 \times 10^{-19}$ J our simulations reach convergence at the latest after ca 10^5 Monte Carlo steps (for details see [14]). With this choice of A_H the van der Waals energy of two equal sized clustered particles at distance $r_{ij}^{\min}$ equals their total kinetic energy at room temperature, $2k_BT$.

In an external magnetic field (uniform magnetic induction B) the total potential energy of a particle i is

$$E_i^{tot}(\vec{r}_i, \vec{\mu}_i) = \sum_{j\neq i}\{E_{ij}^{s} + E_{ij}^{vd\,W} + E_{ij}^{dd}\} - \vec{\mu}_i\vec{B}. \tag{9}$$

We have imposed periodic boundary conditions to avoid edge effects, but the above energy can only be calculated for a finite number of particles j. For the short-range van der Waals interaction it is sufficient to take only particles at distances $r_{ij} \leqslant r_C = 7R_i$ into account (a further increase did not change the results, see also [42]). Dipole–dipole interaction, however, is long-range and thus the interaction with particles at distances $r_{ij} > r_C$ is evaluated using the so-called reaction field method (at large distances the sample is treated as a homogeneous medium interacting with all particles at $r_{ij} < r_C$ via a so-called reaction field, B_R). In this approach [43–45]

$$E_i^{tot} \simeq \sum_{\substack{j\neq i \\ r_{ij}<r_C}}\{E_{ij}^{s} + E_{ij}^{vd\,W} + E_{ij}^{dd}\} - \vec{\mu}_i(\vec{B}_R^i + \vec{B}) \tag{10}$$

holds with

$$\vec{B}_R^i = \frac{2(\mu_{eff} - 1)}{2\mu_{eff} + 1}\cdot\frac{\mu_0}{4\pi r_C^3}\sum_{\substack{j \\ r_{ij}<r_C}}\vec{\mu}_j. \tag{11}$$

The effective permeability, μ_{eff}, depends on the total magnetization of the simulation cell of volume L^3, so that

$$\mu_{eff} = 1 + \frac{\mu_0}{B}\cdot\frac{|\sum_{k=1}^{N}\vec{\mu}_k|}{L^3}. \tag{12}$$

The sum of all dipole moments is calculated self-consistently in every Monte Carlo step, whereas at $B = 0$ we use an extrapolated value.

4.2. Size and shape of clusters

An example of an equilibrium configuration is shown in figure 7. The data are consistent with 2D-SAXS results (not shown, see [14]). Already at zero field there are clusters of particles, but the microstructure is isotropic. Most of the larger particles with high dipole moments are found to belong to clusters. Nevertheless, clusters also contain small particles (for a statistical analysis we refer to [14]). At saturation magnetization, $B = 0.3\,\mathrm{T}$, chain-like structures are clearly visible. These clusters are oriented with their longer axis parallel to the applied field.

For a quantitative analysis we have to define at which distance two particles can be considered as clustered. As described above, the surfactant molecules are not rigid rods (section 4.1 and figure 6), so that particles can form clusters in a range of distances, a fact that is confirmed by TEM studies [24]. The minimum distance, $r_{ij}^{\min}$, has been defined above (equation (5)). The maximum distance of clustered particles is limited by the length of the spacer molecules forming the surfactant layer, i.e. $r_{ij}^{\mathrm{cluster}} \leqslant (R_i + R_j) + 2 \cdot 2\,\mathrm{nm}$ holds. Once again, it will depend on the microscopic details (tilt, entanglement, inter-penetration) below which distance two particles can be considered as clustered (see the description in section 4.1). In the following, we consider two particles as clustered when for their centre-to-centre distance, r_{ij},

$$r_{ij}^{\min} = 1.1(R_i + R_j) \leqslant r_{ij} \leqslant 1.2(R_i + R_j) = r_{ij}^{\mathrm{cluster}} \qquad (13)$$

holds. For the biggest particles in our simulation, $R_i = R_j = 10\,\mathrm{nm}$ this corresponds to a maximum surface-to-surface distance of 4 nm, i.e. twice the length of the spacer molecules. Small particles have a stronger surface curvature and thus a lower average surface density, so that they can come closer to each other. Note that the actual particle distances are found as a result of many Monte Carlo steps involving all interaction energies. Thus the above equation does not pre-determine particle distances but is used only as a tool allowing us to count clusters once an equilibrium configuration has been found.

With the above definition, we can perform a statistical analysis of clusters. In order to guarantee a sufficiently good statistical representation of particle size distribution and spatial configuration, we average over an adequate number of simulation cells, so that the total number of particles simulated is about 3500, even at low filling factors. Depending on the filling factor (2.4–15%) we find 20–80% of the particle mass in clusters, whereas the agglomeration degree increases with the particle concentration. There is only a small field dependence, which we do not discuss here (for details see [14]). Most of these clusters consist of only a few particles. This is shown in figure 8, where we display the probability, $p(s)$, that a particle belongs to a cluster of s particles ($s = 1, 2, \ldots$ and $\sum_s p(s) = 1$). It is evaluated by counting the number of particles found in s-particle clusters, N_s, and dividing it by the total number of all particles in a sample, N. The higher the particle concentration (volume filling factor f), the larger

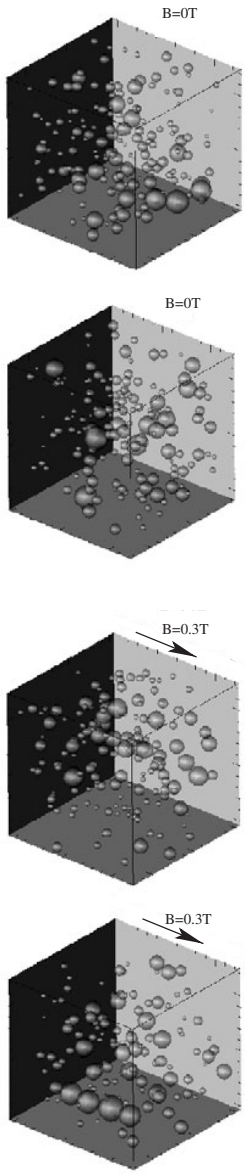

Figure 7. Monte Carlo simulation of a polydisperse ferrofluid (EMG 911 with filling factor 2.4 vol.%). An external magnetic field ($B = 0.3\,\mathrm{T}$) induces formation of anisometric clusters, i.e. chain-like structures with a preferred orientation parallel to B.

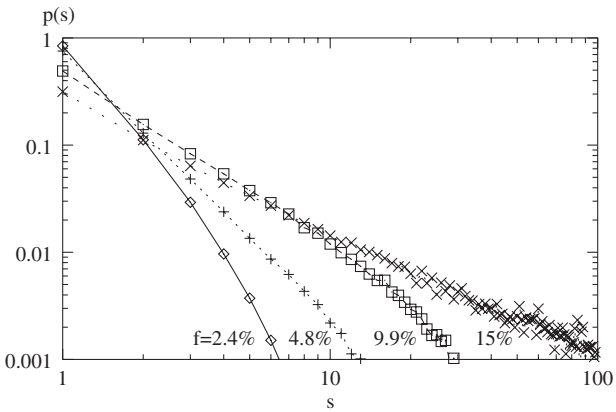

Figure 8. The probability that a particle belongs to a cluster of s particles for $B = 0.3\,\mathrm{T}$. The case $s = 1$ corresponds to single particles.

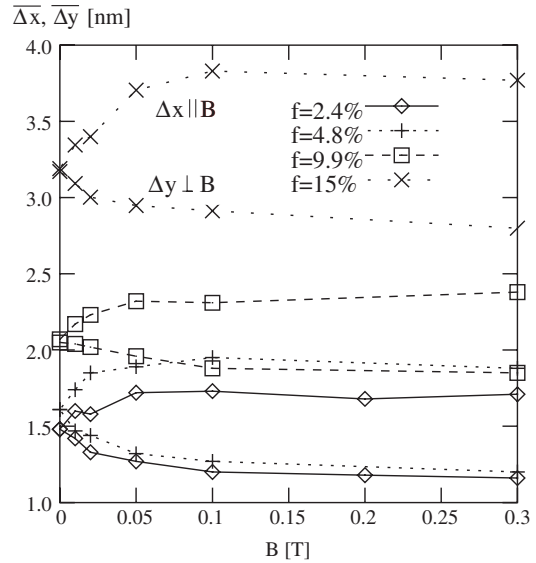

Figure 9. Volume-weighted cluster elongations vs magnetic induction. For every sample the respective upper curve corresponds to elongations $\overline{\Delta x}$ parallel to the applied field, $B = B_x$, while the lower curve shows elongations $\overline{\Delta y}$ perpendicular to B. With increasing field shape anisometry develops: $\overline{\Delta x} > \overline{\Delta y}$. The higher the particle concentration, the higher the cluster elongations.

the number of big the clusters that can form. At $f = 15\%$ there are even clusters with more than 100 particles.

In order to characterize the average shape of clusters in a simple way, we evaluate their elongation parallel (Δx) and perpendicular (Δy) to the field axis. Since we have to take the irregularity of cluster forms into account, the respective contributions of clustered particles are volume-weighted. In the field direction, this reads for a given cluster

$$\Delta x = \frac{\sum_{j=1}^{s} |x_j - x_c| V_j}{\sum_{j=1}^{s} V_j}, \tag{14}$$

where $s \geqslant 2$ is the number of particles belonging to the cluster, x_j and V_j denote position and volume of particle j and $x_c = \sum_{j=1}^{s} x_j V_j / \sum_{j=1}^{s} V_j$ is the coordinate of the cluster's centre of gravity along the field axis $\hat{x}$. Δy is calculated correspondingly. These volume-weighted elongations are not to be confused with the absolute extension of a cluster. In figure 9 we display number-weighted average values $\overline{\Delta x}$ and $\overline{\Delta y}$ for our samples. The higher the particle concentration the bigger the clusters. At zero field $\overline{\Delta x} = \overline{\Delta y}$ holds; i.e. single clusters that are surely not isometric (perfectly spherical) have a random orientation. With increasing magnetic field, $\overline{\Delta x}$ increases while $\overline{\Delta y}$ decreases. This is partly due to an alignment of clusters in the field direction. In addition, there is a re-arrangement of particle positions in clusters.

5. Dielectric spectroscopy: structural changes and dielectric anisotropy

5.1. A short discussion of spectra at zero magnetic field

Finally, we have performed dielectric measurements on the samples listed in table 1 [19,46,47]. The complex permittivity

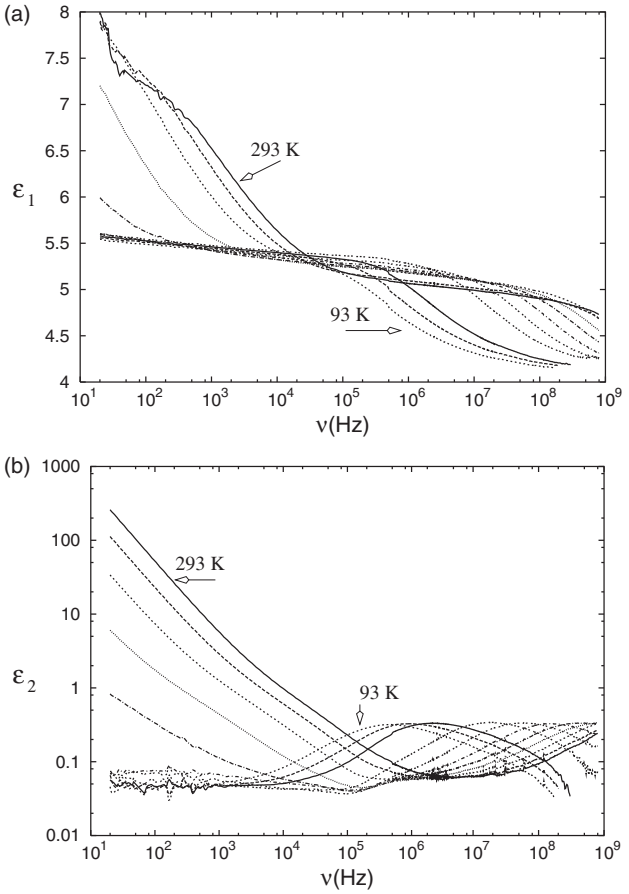

Figure 10. Real and imaginary parts of permittivity vs frequency for sample EMG 900 ($f = 19\%$) at various temperatures (in steps of 20 K). (*a*) ε_1: semi-log plot; (*b*) ε_2: double-log plot.

$\varepsilon = \varepsilon_1 - i\varepsilon_2$ was measured using a broadband transmission method covering the frequency range from 5 Hz to 1 GHz with a single sample holder [48]. The temperature was varied between 93 and 293 K. Figure 10 shows typical spectra for the ferrofluid with the highest particle concentration. At high temperatures (213–293 K) and low frequencies, the imaginary part reveals the ionic conductivity of the carrier liquid ($\varepsilon_2 \propto \sigma/\nu$). In addition, there is a corresponding electrode polarization process (high values of ε_1 below 10 kHz). When the temperature is lowered the conductivity decreases and a high-frequency process shifts into the accessible frequency window. At temperatures between 193 and 213 K the carrier liquid freezes. Therefore, the aforementioned low-frequency losses disappear and only the high-frequency process remains visible. This is more clearly shown in figure 11 for $T = 98$ K. In the following, we want to discuss briefly the underlying polarization mechanisms.

The ferrofluid samples consist of conductive magnetite particles dispersed in a carrier liquid, Isopar-m. Additional measurements on this liquid reveal a permittivity of $\varepsilon_m \simeq 2.28$, but there are no losses at temperatures below 210 K. The same holds for the surfactant layer of spacer molecules: measurements on bulk oleic acid show a constant permittivity $\varepsilon_{surf} \simeq 2.8$ but no losses. The low-frequency losses we observe in the ferrofluids (see figure 10 below 10^5 Hz) are not due to the bulk properties of liquid and surfactant. They

are mainly caused by mobile ions in the carrier liquid. Additional contributions might come from unknown additives the manufacturer did not specify or from ions chemisorbed to the surfactant shell (according to [49–51] the latter process may lead to formation of an electric double layer). We shall analyse these low-frequency losses in a further paper since they are not relevant in the context of field-dependent structure formation. In the following we only discuss either complete spectra at low temperatures or high-frequency data ($\nu \geqslant 10^5$ Hz), i.e. the range where the aforementioned low-frequency processes are not present. Since both the carrier liquid and the surfactant have a similar dielectric response, we cannot distinguish between them and treat them as a single homogeneous and loss-free matrix.

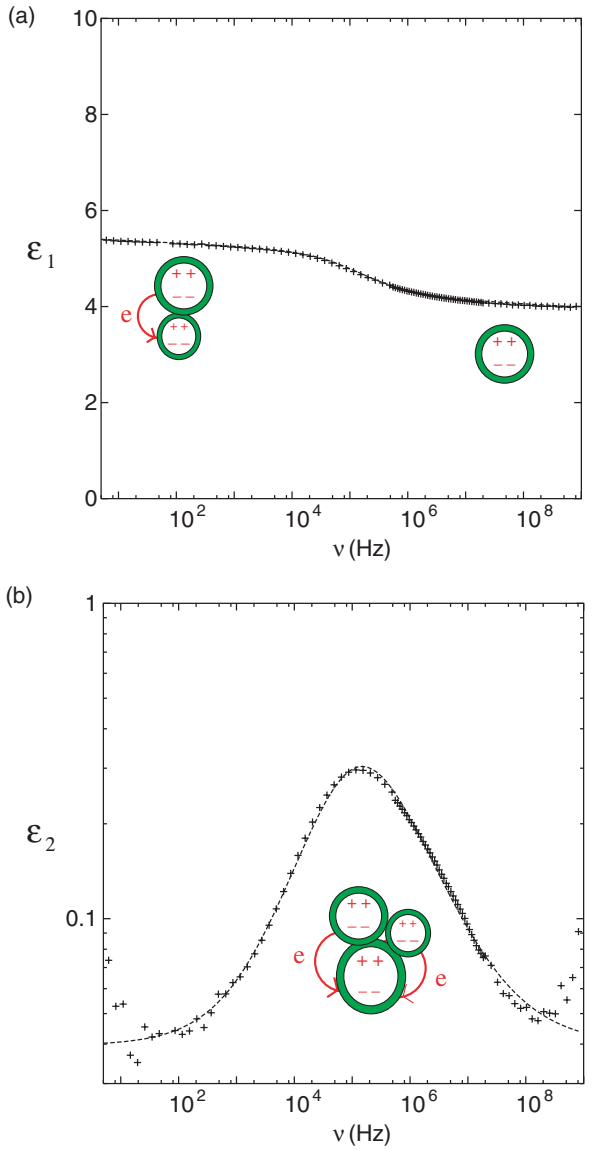

Figure 11. Real and imaginary parts of permittivity vs frequency for sample EMG 900 ($f = 19\%$) at $T = 98$ K. (*a*) ε_1: semi-log plot; (*b*) ε_2: double-log plot. The insets refer to the respective polarization mechanism: interfacial polarization of single particles at high frequencies and additional cluster polarization at low frequencies. The latter process is due to charge carrier hopping between clustered particles.

According to the above remarks, we can expect that at low temperatures all remaining significant polarization processes are related to the fact that the dispersed particles are conductive. In an electric field, the particles become polarized, resulting in an enhanced permittivity compared with that of the pure matrix (interfacial-polarization process or Maxwell–Wagner–Sillars polarization). According to effective medium theory this holds in the frequency range below a characteristic frequency, ν_{pol}, characterizing a decay of polarization [6,7]. ν_{pol} is proportional to the conductivity of the particles. An estimate yields for its order of magnitude (see equation (11) of [4]):

$$\mathrm{O}(\nu_{\mathrm{pol}}) = \frac{(1/3)(1-f)\sigma}{2\pi\varepsilon_0\varepsilon_{\mathrm{m}}} = \left(\frac{6\cdot(1-f)}{\varepsilon_{\mathrm{m}}}\mathrm{GHz}\right) \times(\sigma \text{ in } \mathrm{S\,m^{-1}}). \tag{15}$$

The dc-conductivity of bulk magnetite is about $100\,\mathrm{S\,m^{-1}}$, so that ν_{pol} should be of the order of 10^{11} Hz. In other words, in our measurement range up to 1 GHz, the polarization of single particles can only yield a frequency-independent enhancement of permittivity. Obviously, there is an additional mechanism at lower frequencies (see figure 11). But at first, let us focus on the single-particle polarization characterizing the high-frequency limit of our spectra: there are various effective medium approximations describing the increase of permittivity with particle concentration (volume filling factor, f) [6,7]. In [12] we could show that for randomly distributed monodisperse spheres the Maxwell–Garnett formula is not just a dilute limite approximation but exact. In contrast, polydisperse spheres having a sufficiently broad distribution of particle sizes (such as our ferrofluids, see figure 2), are satisfactorily well described by the Hanai–Bruggeman formula. At quasi-static frequency it reads

$$\varepsilon_1(\nu \ll \nu_{\mathrm{pol}}) = \frac{\varepsilon_{\mathrm{m}}}{(1-f)^3}, \tag{16}$$

where ε_{m} denotes the permittivity of the matrix (in our case that of the carrier liquid, $\varepsilon_{\mathrm{m}} = 2.28$). Figure 12 shows that there is a good agreement between this model and the experimental values $\varepsilon_{\mathrm{hf}} = \varepsilon_1(\nu = 1\,\mathrm{GHz})$. This shows that at high frequencies we indeed observe interfacial polarization of single particles having a broad size distribution.

Consequently, the observed increase of ε_1 at low frequencies and the corresponding loss peak (see figure 11) must be due to another transport mechanism that is still active at low temperatures. As already mentioned, it has to be related

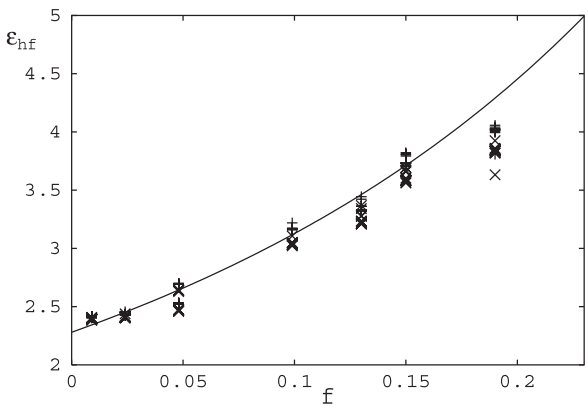

Figure 12. High-frequency permittivity vs volume filling factor f.

to the fact that the particles are conductive. The strength of the process, $\Delta\varepsilon = \varepsilon_{\text{static}} - \varepsilon_{\text{hf}}$, increases with increasing particle concentration. Below 110 K the thermal activation of the peak frequency deviates from Arrhenius behaviour and can be described using models for charge hopping (not shown; for details we refer to [46]). Since the lowest interparticle distances occur in clusters, it seems reasonable to interpret the observed loss peak via charge carrier hopping between clustered particles (see insets in figure 11). Thus, at low frequencies polarization of both single particles and clusters contribute to the measured permittivity. Note that effective medium theories in general neglect charge hopping between spatially separated particles (matrix inclusion topology). Therefore, in ferrofluids a comparison of dielectric low-frequency data with effective medium formulas is not possible.

Summarizing, at temperatures below 210 K the spectra are governed by interfacial polarization of single particles and charge hopping between clustered particles. Single particle polarization determines the high-frequency permittivity, ε_{hf}, whereas the hopping process leads to an increase of permittivity at low frequencies, $\varepsilon_{\text{static}} = \Delta\varepsilon + \varepsilon_{\text{hf}}$.

5.2. Dielectric measurements for $B > 0$: the magnetodielectric effect

As we have shown in sections 3 and 4, ferrofluids develop an anisotropic microstructure when a magnetic field is applied. In order to study the corresponding change of permittivity, we have measured ε for two directions of the electric field, E, i.e. parallel and perpendicular to the magnetic field (see figure 7). Since the carrier liquid freezes below 210 K making field-induced structural changes impossible, we have monitored different cooling cycles with and without a magnetic field. The result is displayed in figure 13, where we compare measurements at $B = 0$ with those at saturation induction, $B = 0.3$ T. We observe field-induced dielectric anisotropy, i.e. an increase of ε for $E \parallel B$ and a decrease of ε for $E \perp B$. The anisotropy is stronger at low frequencies, reaching a relative difference of permittivity $(\varepsilon_{\vec{E}\parallel\vec{B}} - \varepsilon_{\vec{E}\perp\vec{B}})/\varepsilon_{B=0}$ of ca 22–23% compared with ca 8–9% at high frequencies (for $f = 19\%$). This means that the field-induced change of microstructure

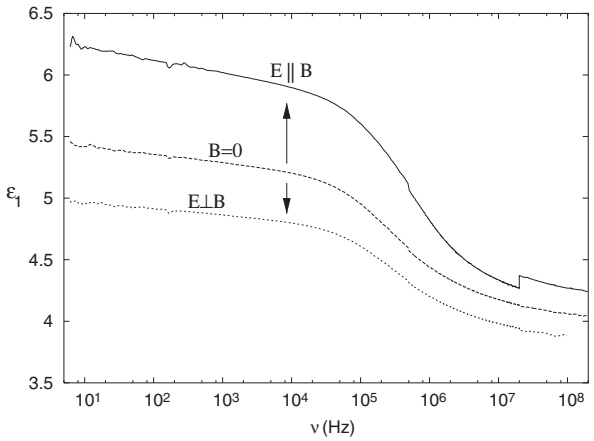

Figure 13. Semi-log plot of ε_1 vs frequency for sample EMG 900 ($f = 19\%$) at $T = 123$ K.

affects both the interfacial polarization of particles as well as the charge hopping between clustered particles.

Before continuing the analysis of experimental data, we would like to get an estimate as to what extent the observed anisotropy might be due to field-induced orientation of single non-spherical particles. As already mentioned, the magnetite particles are not perfect spheres but can be described on an average as ellipsoids with an effective axis ratio of 1.05 (see [13]). For oriented particles equation (16) changes to

$$\varepsilon_{1,i}(\nu \ll \nu_{\text{pol}}) = \frac{\varepsilon_{\text{m}}}{(1-f)^{1/A_i}}, \tag{17}$$

where A_i denotes the corresponding depolarization factor in direction i of the electric field (see equation (27a) in [3] for $|\varepsilon_2| \to \infty$). An axis ratio of 1.05 corresponds to $A_\parallel \simeq 0.32$ for $\varepsilon_{\vec{E}\parallel\vec{B}}$, whereas $A_\perp \simeq 0.34$ for $\varepsilon_{\vec{E}\perp\vec{B}}$ [52]. For a random orientation at zero magnetic field the average depolarization factor is $A \simeq \frac{1}{3}$, i.e. it equals that for spheres ($1/A = \frac{1}{3}(2/A_\perp + 1/A_\parallel)$, see [3]). Therefore, at $f = 19\%$ single-particle orientation should yield a relative change of the order of $(\varepsilon_{\vec{E}\parallel\vec{B}} - \varepsilon_{\vec{E}\perp\vec{B}})/\varepsilon_{B=0} \simeq 3.9\%$. A comparison with the measured change of 8–9% in ε_{hf} clearly shows that there must be an additional structural change, i.e. formation of anisometric clusters. Moreover, the latter effect must be dominant at low frequencies, where we have even measured an anisotropy of 22% (at $f = 19\%$).

Next, we investigate the development of anisotropy choosing a reference frequency of 1 MHz. At room temperature this frequency is below the characteristic frequency of the hopping process, so that we monitor quasi-static low-frequency data in figure 14(a) (single particle and cluster polarization). The field-dependence of permittivity is similar to that of the cluster elongations determined by Monte Carlo simulations (compare figures 14(a) and (b)). Obviously, the oriented chain-like clusters contribute much more strongly to the measured effective permittivity when the electric field is parallel to their longer axis, $\vec{E} \parallel \hat{x}$ (see figure 7). This can be qualitatively explained using a rather simple model: (a) in terms of single particle polarization—a series circuit of conducting and insulating layers (particles separated by surfactant layers) gives rise to a higher polarization and permittivity than a parallel circuit; (b) in terms of cluster polarization due to hopping—the probability that a particle has a neighbour in the direction parallel (perpendicular) to the chain axis is higher (lower) than in isometric clusters at $B = 0$.

Summarizing, field-induced structural anisotropy reflects in dielectric anisotropy. According to figure 14 dielectric measurements can be used to monitor the chain formation in ferrofluids.

6. Conclusions

We have shown how an external magnetic field induces anisotropy in ferrofluids containing polydisperse nanoparticles. The change of microstructure is due to formation of anisometric clusters having a preferred orientation parallel to the field. 2D-SAXS reveals that particles of all sizes take part in cluster formation. Since magnetic dipole–dipole interaction is much stronger for large particles, this experimental result underlines the importance of van der Waals interaction

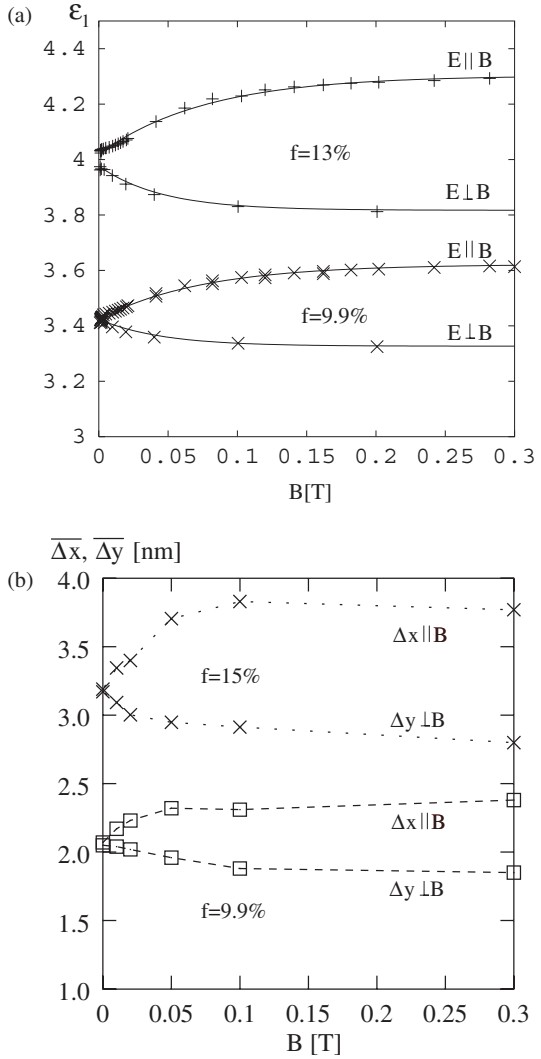

Figure 14. (*a*) Measured real part of permittivity at $\nu = 1$ MHz vs magnetic induction at $T = 293$ K for samples EMG 905 ($f = 9.9\%$) and EMG 901 ($f = 13\%$). Values for electric fields $\vec{E} \parallel \vec{B}$ and $\vec{E} \perp \vec{B}$ are displayed. (*b*) Monte Carlo-simulations of volume-weighted cluster elongations in the direction of the applied magnetic field ($\overline{\Delta x}$) and perpendicular to it ($\overline{\Delta y}$) for samples EMG 905 and EMG 901a.

for the thermal stability of clusters. Monte Carlo simulations have revealed size distribution and shape anisometry of the clusters. We have compared the structural data with results from broadband dielectric measurements. At low temperatures the dielectric response is governed by interfacial polarization of single particles and clusters. The aforementioned field-induced changes of the spatial arrangement of particles result in dielectric anisotropy, i.e. in an enhancement of permittivity for $\vec{E} \parallel \vec{B}$ and a decrease of permittivity for $\vec{E} \perp \vec{B}$. This behaviour is correlated with the respective cluster elongations: oriented chain-like clusters contribute much more strongly to the measured effective permittivity when the electric field is parallel to their longer axis, $\vec{E} \parallel \hat{x}$, and vice versa. In addition, the re-orientation of single non-spherical particles also yields a small contribution to the observed anisotropy.

Acknowledgments

The authors are grateful to Prof. Dr Günter Nimtz for hosting this work in his laboratory. The project was supported by the European Commission under TMR Marie Curie Grant No ERBFMBICT982913 (A.S.) and by the DFG under Project No Ni/49/33-1.

References

[1] Pelster R and Nitsch J 2002 *Kleinheubacher Berichte* vol 45 (Darmstadt: T-Systems) ISSN 0343-5725 pp 312–19
Pelster R and Nitsch J 1999 *Proc. Int. Symp. Electromagnetic Compatibility (Magdeburg)* ed Nitsch/Wollenberg (Otto-von-Guericke Universität Magdeburg, ISBN 3-929757-25-7) pp 171–78
[2] Monecke J 1989 *Phys. Status Solidi* b **154** 805–13
[3] Bánhegyi G 1986 *Colloid Polym. Sci.* **264** 1030–50
[4] Pelster R and Simon U 1999 *Colloid Polym. Sci.* **277** 2–14
[5] Pelster R 1999 *Phys. Rev.* B **59** 9214–28
[6] van Beek L K H 1967 *Progress in Dielectrics* vol 7, ed J B Birks (London: Heywood) pp 69–114
[7] Dukhin S S 1986 *Surface Colloid Science* vol 3, ed E Matijevic (New York: Interscience) p 83–165
[8] Günther K and Heinrich D 1965 *Z. f. Phys.* **185** 345
[9] McKenzie D R, McPhedran R C and Derrick G H 1978 *Proc. R. Soc. Lond.* A **362** 211–32
[10] Harfield N 1999 *Eur. Phys. J. AP* **6** 13–21
Harfield N 2000 *J. Mater. Sci.* **35** 5809–16
[11] Fu L, Macedo P M and Resca L 1993 *Phys. Rev.* B **47** 13818–29
[12] Spanoudaki A and Pelster R 2001 *Phys. Rev.* B **64** 064205
[13] Kruse T, Krauthäuser H-G, Spanoudaki A and Pelster R 2003 *Phys. Rev.* B **67** 094206
[14] Kruse T, Spanoudaki A and Pelster R 2003 *Phys. Rev.* B **68** 054208
[15] Rosensweig R E 1985 *Ferrohydrodynamics* (New York: Cambridge University Press)
[16] Odenbach S (ed) *Ferrofluids, Magnetically Controllable Fluids and their Applications 2002* (*Lecture Notes in Physics* vol 594) (Berlin: Springer)
[17] Kaplan B Z and Jacobson D M 1976 *Nature* **259** 654
[18] Mailfert A J and Nahounou B 1980 *IEEE Trans. Magn.* **MAG-16** 254
[19] Spanoudaki A and Pelster R 2002 *J. Magn. Magn. Mater.* **252** 71–3
[20] Davies H W and Llewellyn J P 1980 *J. Phys. D: Appl. Phys.* **13** 2327
[21] Yusuf N A, Ramadan A and Abu-Safia H 1998 *J. Magn. Magn. Mater.* **184** 375
[22] da Silva M F and Figueiredo Neto A M 1993 *Phys. Rev.* E **48** 4483
[23] Stevens M J and Grest G S 1994 *Phys. Rev. Lett.* **72** 3686
Stevens M J and Grest G S 1995 *Phys. Rev.* E **51** 5962
Stevens M J and Grest G S 1995 *Phys. Rev.* E **51** 5976
[24] Popplewell J and Sakhnini L 1995 *J. Magn. Magn. Mater.* **149** 72
[25] Kruse T 2000 *PhD Thesis* (Universität zu Köln)
[26] Kneller E 1962 *Ferromagnetismus* (Berlin: Springer)
[27] Staude H (ed) 1945 *Physikalisch-Chemisches Taschenbuch* (Leipzig: Akademische Verlagsgesellschaft)
[28] Kaizer R and Miscolczy G 1970 *J. Appl. Phys.* **42** 1064
[29] Johansson C, Hansson M, Pedersen M S and Morup S 1997 *J. Magn. Magn. Mater.* **173** 5
[30] Krauthäuser H-G and Nimtz G 1996 *J. Mol. Struct.* **383** 315
[31] Krauthäuser H-G 1996 *PhD Thesis* (Universität zu Köln)
[32] Haubold H-G *et al* 1989 *Rev. Sci. Instrum.* **60** 1943
[33] Odenbach S and Störk H 1998 *J. Magn. Magn. Mater.* **183** 188
[34] Morozov K I 2002 *Phys. Rev.* E **66** 011704

[35] Pshenichnikov A F and Mekhonoshin V V 2001 *Eur. Phys. J.* E **6** 399–407
[36] Cabral B J C 2000 *J. Chem. Phys.* **112** 4351
[37] Metropolis N, Rosenbluth A W, Rosenbluth M N, Teller A H and Teller E 1953 *J. Chem. Phys.* **21** 1087
[38] Israelachvili J N 1985 *Intermolecular and Surface Forces* (San Diego: Academic)
[39] Mahanty J and Ninham B W (ed) 1976 *Dispersion forces* (New York: Academic)
[40] Bergström L 1997 *Adv. Colloid Interface Sci.* **70** 125
[41] Donselaar L N, Frederik PM, Bomans P, Buining P A, Humbel B M and Philipse A P 1999 *J. Magn. Magn. Mater.* **201** 58
[42] Andersson J-O, Djurberg C, Jonsson T, Svedlindh T and Nordblad P 1997 *Phys. Rev.* B **56** 13983
[43] Barker J A and Watts R O 1973 *Mol. Phys.* **26** 789
[44] Friedman H L 1975 *Mol. Phys.* **29** 1533
[45] Barker J A 1980 *NRCC Workshop Proc.* vol 9, pp 45–46
[46] Spanoudaki A 2002 *PhD Thesis* Universität zu Köln
[47] Spanoudaki A, Kruse T, Pelster R and Nimtz G 1999 *Proc. 10th Int. Symp. on Electrets, ISE 10 (Delphi, Greece)* (IEEE 99CH36256, ISBN 0-7803-5025-1) pp 679–82
[48] Pelster R 1995 *IEEE Trans. Microwave Theory Tech.* **43** 1494–501
[49] Schwarz G 1962 *J. Phys. Chem.* **70** 2636
[50] Radulescu M M 1990 *J. Magn. Magn. Mater.* **85** 144
[51] Malaescu I and Marin C N 2002 *J. Colloid Interface Sci.* **251** 73
[52] Osborn J A 1945 *Phys. Rev.* **67** 351–7